Tribology International 162 (2021) 107108

Contents lists available at ScienceDirect

Tribology International

journal homepage: www.elsevier.com/locate/triboint

Tracing single asperity wear in relation to macroscale friction during running-in

Feng-Chun Hsia [a,b,1], Fiona M. Elam [a,b,1], Daniel Bonn [b], Bart Weber [a,b,*], Steve E. Franklin [a,c,*]

[a] Advanced Research Center for Nanolithography (ARCNL), Science Park 106, 1098XG Amsterdam, The Netherlands
[b] Van der Waals-Zeeman Institute, IoP, University of Amsterdam, Science Park 904, 1098XH Amsterdam, The Netherlands
[c] Department of Materials Science and Engineering, The University of Sheffield, Sheffield S1 3JD, UK

ARTICLE INFO

Keywords:
Multi-asperity contact
Hard material wear
Friction
Boundary element method

ABSTRACT

The running-in wear of a multi-asperity silicon carbide sphere-on-silicon flat interface is investigated at the micro- and nanoscale in relation to the friction behaviour of an unlubricated macroscale tribological system sliding in a unidirectional mode. Experiments and contact simulations indicated that the macroscale friction behaviour during running-in was governed by the wear behaviour of roughness asperities on the sphere and their influence on the interfacial contact pressure. Specific ploughing tracks on the flat corresponded to individual asperities on the sphere which, when worn-off, led to lower, more stable friction behaviour and mild wear at an atomic attrition-like rate. It was also found that single asperity contact simulations are unable to reliably predict multi-asperity friction and wear behaviour for this system.

1. Introduction

Friction and wear of macroscopic dry sliding contacts are known to have a substantial detrimental impact upon the global energy consumption, economy and environment [1,2]. As a consequence, this has sparked significant scientific interest, with the aim to manipulate and reduce friction and wear of materials under conditions of industrial relevance [3–6]. Friction and wear behaviour at the macroscopic length scale is typically influenced by the topography of the contacting surfaces [7]. The real area of contact consists of numerous micro- and nanoscale contacts – the result of contacting asperities – that together with the shear strength occurring at these individual contacts, determines the overall friction. The initial surface topography is known to have its greatest effect at the outset of sliding, during the tribological process known as 'running-in' where plastic deformation or fracture of roughness asperities can occur, rather than during the subsequent period [8]. Advancing the scientific understanding of the mechanisms behind the running-in process can lead to optimisation and stabilisation of the working performance of engineering tribosystems, thus extending their lifetime [9]. Running-in can be considered in terms of a collection of macro-, micro-, and nanoscale processes that occur both simultaneously and sequentially [9]. Since these processes occurring on different length scales are all hidden at the contact interface, they are particularly challenging to access experimentally. It is therefore unsurprising that the running-in process is poorly understood.

In order to simplify the tribological system, fundamental studies into the isolated friction and wear events occurring at a single asperity during the onset of dry sliding have attracted considerable attention, with the intention to collectively transform the outcomes into 'multi-asperity' level behaviour at the macroscale [7–16]. Single asperities are known to undergo truncation: relatively sharp fresh, unworn surfaces are reduced to a state of surface conformity at the microscale, as a result of the concentrated stresses occurring at the ends of the highest interacting asperities [8]. The running-in friction behaviour of the single asperity tribological systems studied by Bhaskaran et al [12]. and Gotsmann et al [13]. (represented graphically as $y \propto \sqrt{x}$, where y = coefficient of friction and x = sliding distance) were characteristic of a dry sliding system where a small amount of surface contamination, oxide or adsorbed species at the interface is quickly worn away to cause a greater degree of adhesion and a rise in friction [9]. In their investigations, the effect of counter surface wear was minimised, and the asperity wear attributed to atom-by-atom attrition [12,13]. However, when counter surface wear does occur, as in the case reported by Schiffmann et al [15]. and Yu et al [16]. for reciprocating dry sliding systems, single asperity friction is initially found to be controlled by the ploughing friction component in the first few sliding cycles; transitioning to a regime whereby the elastic or adhesion friction component increases and eventually dominates as the number of cycles increase. The running-in

* Corresponding authors at: Advanced Research Center for Nanolithography (ARCNL), Science Park 106, 1098XG Amsterdam, The Netherlands.
E-mail addresses: b.weber@arcnl.nl (B. Weber), s.franklin@arcnl.nl (S.E. Franklin).
[1] Co-first authorship.

https://doi.org/10.1016/j.triboint.2021.107108
Received 13 March 2021; Received in revised form 7 May 2021; Accepted 23 May 2021
0301-679X/© 2021 The Author(s). Published by Elsevier Ltd. This is an open access article under the CC BY license (http://creativecommons.org/licenses/by/4.0/).

friction behaviour in this instance (represented graphically as $y \propto 1/x$, where y = coefficient of friction and x = sliding distance) is characteristic of initially high contact pressures at the sliding interface inducing a rapid transition to the steady state [9]. Bhushan et al. also reported a transition between single asperity ploughing and adhesion friction; noting that with an increase in plastic deformation (ploughing), a greater value of the total friction coefficient was observed [17]. The transition from ploughing to adhesion friction was attributed to the wear occurring at the interacting apex of the contact asperities. The unexpected wear mechanisms that occur at hard contact asperities in a hard-soft sliding pair, have been observed for several different contact systems and attributed to both atom-by-atom attrition and fracturing [18–20].

Despite substantial research effort, it remains unclear exactly how the nano-tribological response of a single asperity during the running-in process would, in reality, translate to that of a more industrially-relevant multi-asperity contact interface. Remarks were made by Yu et al. [21]. in relation to the similarities in contact pressure beneath some asperities in a multi-asperity system and that of a single asperity system, resulting in similar counter surface wear behaviour. However Qi et al. [22]. showed that a glass-on-silica system demonstrated opposing trends for single and multi-asperity contacts in relation to the system friction behaviour under humid and dry conditions. The combination of the single asperity perspective with a macroscale multi-asperity tribological system has been reported by Krick et al. [23]. and Garabedian et al. [24]. where single asperity wear was traced at sub-micrometre resolution utilising white light interferometry, to investigate a reciprocated sliding system. The asperity-scale wear behaviour was found to mirror that of macroscale wear, with high wear rates detected during the running-in process, transitioning abruptly to ultra-low wear rates once the system had reached the steady state period [24]. However, no insights into the relationship between the single asperity wear mechanisms and the running-in friction response of the macroscale system were provided. It is conceivable that simply translating the tribological behaviour of single asperity systems into that of a multi-asperity system is not so trivial.

The intention of this work is to highlight the relationship between the wear events occurring at single asperities during the onset of dry sliding and the friction response of a multi-asperity tribological system, with hard-soft sliding pairs where ploughing by the asperities is likely to occur. Investigations into the running-in wear mechanisms of multi-asperity contacts are conducted at the micro- and nanoscale, in relation to the friction behaviour of a macroscale tribological system dry sliding in a unidirectional mode. Focus is placed on the study of industrially-relevant silicon carbide and silicon materials that are typically found in micro-/nano-electromechanical systems MEMS/NEMS [25]. Experimental methods and elastic-full plastic contact calculations are utilised [26], which enable the study of multi-asperity contacting interfaces with single asperity detail, as the system transitions through the initial running-in stage. The choice to apply a 'unidirectional' sliding mode, where the silicon carbide sphere always encounters a pristine silicon surface throughout the sliding measurement, aims to trace the evolution of the asperity friction and wear whilst minimising the formation of third bodies. The latter are known to influence the friction and wear behaviour of this type of tribological system [27].

2. Experimental

2.1. Materials

The two industrially-relevant contact materials selected for study were 3 mm diameter direct sintered silicon carbide (SiC) spheres (Grade 10, DIT Holland) and polished p-type single crystal (100) silicon (Si) wafers (University Wafer) with a native oxide layer. The root mean square roughness measured by AFM (scan size 5 μm × 5 μm) of the pristine multi-asperity SiC sphere and Si flat surfaces were 48.7 nm and 0.9 nm, respectively [27]. The spheres were cleaned prior to use using acetone and isopropanol (Sigma Aldrich) in an ultrasonic bath for 10 min in each solvent; followed by a deionised water rinse. The same cleaning procedure was used for removal of wear debris as indicated.

2.2. Methods

The sphere-on-flat tribological experiments were performed using a universal mechanical tester (UMT Tribolab, Bruker), utilising a 'unidirectional' sliding mode as illustrated in Fig. 1a. An applied load of 100 mN was chosen, with a sliding speed of 0.5 mm s^{-1}, a sliding distance per stroke of 20 mm, and a total sliding distance of 40 mm or 6 m in the case of 'short' or 'long' studies respectively. Experiments were performed in an unregulated ambient environment (20–22 °C; 40–60% relative humidity). Force and position data were acquired at a rate of 5 Hz. Each 6 m sliding experiment was repeated three times with pristine samples, with data presented as a moving average (over two strokes and for the three independent repeat experiments).

To characterize the wear of the contacts, optical focus variation profilometry measurements were performed *ex-situ* using a laser scanning confocal microscope (VK-X1000, Keyence). Similarly, the surface topography of the contacts was measured using atomic force microscopy (AFM) (Dimension Icon, Bruker) implemented in tapping mode, using a silicon tip with a radius of approximately 8 nm (RTESPA-300, Bruker). Images were processed using Gwyddion software [28], and MATLAB. All reported route mean square (RMS) roughness values for the Si flat were based on AFM scan sizes of 45 μm × 2.8 μm (1024 × 64 pixels); and for the SiC sphere were based on the worn area highlighted in Fig. 1. The wear tracks on the Si flats were additionally imaged and analysed using scanning electron microscopy (Verios 460, FEI) and integrated energy dispersive X-ray spectroscopy (X-Max EDS, Oxford Instruments).

Contact calculations using the Tribology Simulator that is publicly available at www.tribology.org, were employed to estimate the plastic deformation at the SiC sphere-on-Si flat interface. The half-space contact calculations were based on the boundary element method (BEM) [26], whereby the elasto-plastic deformation of asperities at the interface was solved. In the calculation, strain hardening is assumed to be negligible, and the contact pressure is limited by the hardness of the softest contact material; Si in this study (Table 1). The contact calculations were carried out at 100 mN, utilising height profiles of the SiC sphere measured by AFM (scan size 85 μm × 85 μm; 4096 × 4096 pixels), and the mechanical properties listed in Table 1 as input. This AFM scan size was chosen to ensure it was considerably larger than the Hertzian contact diameter of ~20 μm under the conditions used.

3. Results and discussion

3.1. Running-in friction and wear response at the macroscale

Fig. 1 shows the typical running-in friction and wear outcome for unidirectional sliding of a multi-asperity SiC sphere-on-Si flat system over a total distance of 40 mm, demonstrating evidence of counter surface ploughing and hard contact asperity wear. The friction over the 40 mm sliding distance illustrated in Fig. 1b, shows initially high and irregular behaviour with a friction coefficient (CoF) peak at 0.63 at the onset of sliding, and a relatively sudden decline to a more stable CoF of 0.31 at ~15 mm. The friction behaviour of the system is directly correlated with the appearance and predominant disappearance of abrasive wear tracks on the Si flat (Fig. 1c); mirroring the total wear track cross-sectional area measured by AFM of tracks 1 and 2, as a function of sliding distance. The behaviour of this multi-asperity system, although more erratic, follows the single asperity running-in friction behaviour reported elsewhere, where the running-in stage is represented graphically as $y \propto 1/x$ (where y = CoF and x = sliding distance) [15,16]. This stage is characterised by high initial contact pressures, counter surface wear, and the total friction response being controlled by a ploughing friction component at the onset of sliding, transitioning to a

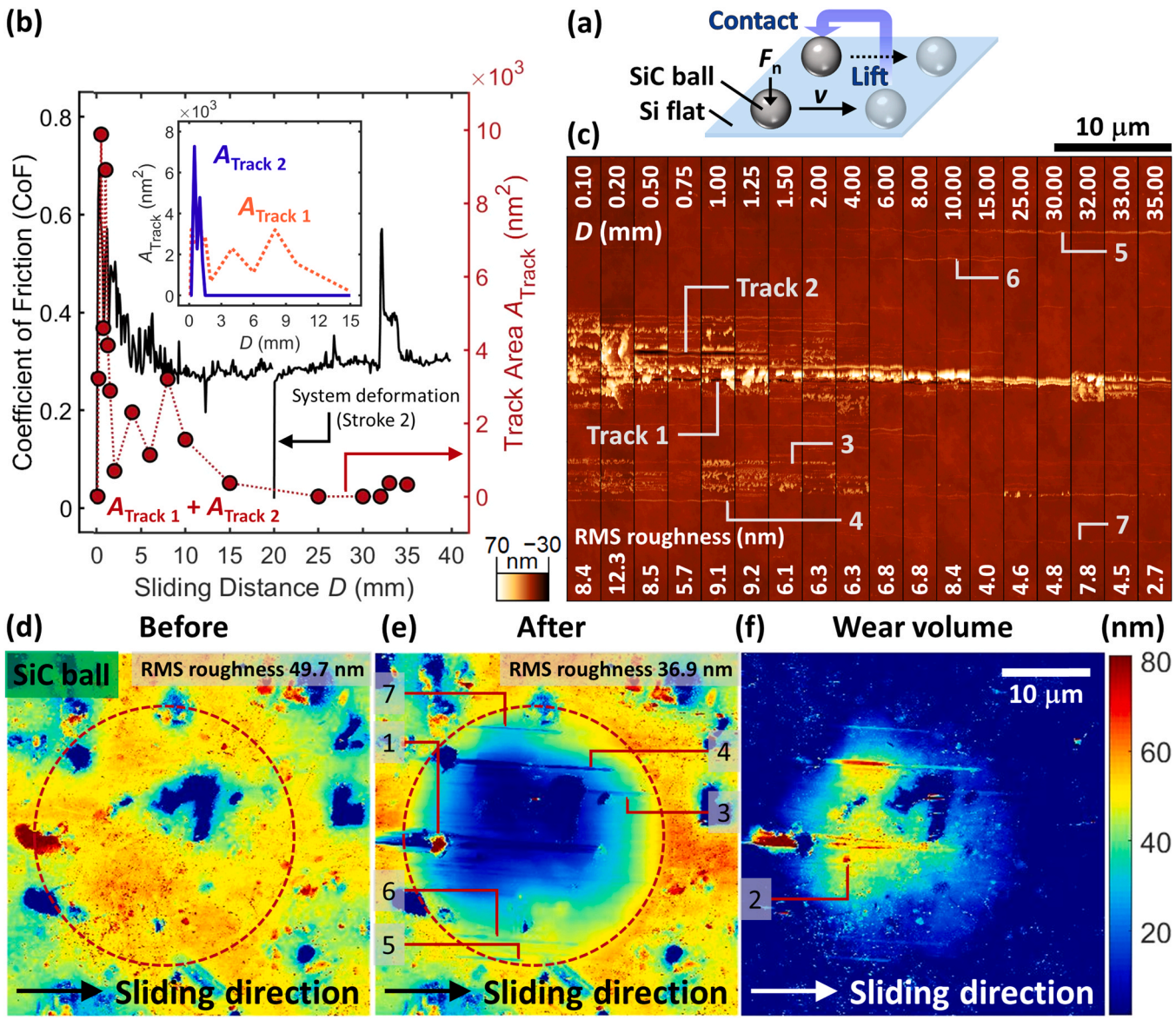

Fig. 1. Friction and wear analysis for unidirectional sliding of a multi-asperity silicon carbide (SiC) sphere-on-silicon (Si) flat over 40 mm distance: (a) schematic illustration of unidirectional sliding mode. (b) Coefficient of friction (CoF) and total wear track cross-sectional area as a function of sliding distance. Inset figure shows the individual cross-sectional area evolution of wear tracks 1 and 2 as a function of sliding distance. (c) AFM micrographs illustrating the topography of wear tracks on Si flat at set sliding positions. AFM micrographs of SiC sphere (d) prior to sliding, (e) after sliding 40 mm and ultrasonic cleaning. Numbers correspond to possible asperity locations responsible for Si flat wear tracks shown in (c); red circle represents worn area. (f) Wear volume removed (9.48 μm^3) from SiC sphere after 40 mm sliding. (For interpretation of the references to colour in this figure legend, the reader is referred to the web version of this article.)

Table 1
Mechanical properties of contact bodies.

Materials	Young's modulus (GPa)	Poisson's ratio	Hardness (GPa)
SiC sphere	460	0.21	25
Si flat	130	0.2	10

regime whereby the relative contribution from the elastic or adhesion friction component increases and eventually dominates.

Evidence for high initial contact pressures in the multi-asperity system can be found in Fig. 1c, depicting the presence of ploughing tracks i.e. counter surface wear on the Si flat, and in Fig. 1e that shows an AFM micrograph of the flattened topography of the hard SiC sphere after sliding 40 mm, suggesting asperity removal over the course of the sliding experiment. These observations are consistent with the calculated reduction in RMS roughness of both contacts after running-in. According to the Hertzian contact pressure at the pristine SiC sphere-on-Si flat interface (~0.46 GPa), no ploughing should occur as this value is considerably less than the Si flat hardness (Table 1). Conversely, the initial Hertzian contact diameter of ~20 μm, is in line with the experimental observations. Therefore, since roughness asperities are not taken into account in the Hertzian calculation, it can be expected that the initial ploughing tracks and accompanying high friction response are caused by the very high contact pressures exerted beneath the asperities leading to localised plastic deformation of the Si flat at the SiC asperity contact points. The abrupt friction drop suggests asperity removal on the SiC sphere and, similar to the single asperity running-in case, a transition in the friction and wear mechanism from ploughing friction and ploughing wear of the Si flat during the running-in process, to adhesion friction and mild wear of both contacts [15]. The evolution of the real interfacial contact pressures of the multi-asperity system will be discussed in more depth later.

Looking in more detail at the ploughing tracks on the Si flat counter surface, Fig. 1c shows the AFM micrographs from which the cross-sectional areas of tracks 1 and 2 on the Si flat were measured at specific sliding locations. Track 2 can be seen to disappear between 1.25 and 1.5 mm sliding; whilst track 1 still remains after 40 mm. Mounds of Si wear debris (Fig. 2) can be seen located around (and potentially covering) the ploughing tracks, particularly within the first millimetre of sliding. There also is evidence to suggest increased levels of oxygen in the mounds of Si wear debris, (confirmed from EDS analysis, Fig. 2e) signifying the presence of SiO_x, as reported previously by Hsia et al. [27]. The precise origin of the SiO_x is not clear from the present study. The SiO_x could occur as a result of mechanochemical activation of the Si in the presence of oxygen and water (ambient conditions), or it could be an accumulation of the native oxide layer from the Si flat at the ploughing track edge, which has been displaced during the sliding experiment.

3.2. Running-in wear response at the asperity-level

In order to provide insight into which asperities on the SiC sphere were responsible for the ploughing tracks found on the Si flat, and into the nature of the wear events occurring at the sliding interface during the running-in process, AFM micrographs detailing the topography of the sphere before and after sliding 40 mm were obtained (Fig. 1d-f). It is clear that asperities have been removed from the surface of the SiC sphere, evident particularly in Fig. 1f illustrating the wear volume, which was constructed by calculating the difference between Fig. 1d and e. The wear rate over the 'short' initial 40 mm sliding distance was calculated to be 2375 μm^3 $(Nm)^{-1}$. Comparing Fig. 1c-f, it is possible to identify which asperities on the SiC sphere could be responsible for particular ploughing tracks observed on the Si flat. A dominant asperity located at the trailing edge (the left edge) of the SiC sphere labelled '1′, is likely responsible for track 1 that remains visible on the Si flat until the end of the 40 mm sliding distance. This asperity appears to evolve from the high feature that lies at the trailing edge of the contact region shown in Fig. 1d. However, more challenging to locate is the asperity responsible for track 2 shown in Fig. 1c that ends abruptly after about 1.25 mm sliding. By analysing track distances with respect to one another, and the SiC sphere orientation during sliding, the asperity potentially responsible for creating this track can be found in the SiC wear volume, Fig. 1f. It is likely that this asperity is not long-lived, given the short wear track it creates on the Si flat and the absence of a clear wear channel on the SiC sphere. Closer inspection of the SiC sphere in fact highlights several wear channels (Fig. 1e), matching the locations of the four shallower wear tracks on the Si flat: tracks 3–7 (Fig. 1c). It is plausible that these wear channels on the SiC sphere originate from asperities at the leading edge that have subsequently fractured off and become wear particles trapped at the contact interface between the sphere and the flat, thus interacting with and wearing both surfaces simultaneously along the sliding direction. This sudden fracturing and trapping of asperities could also account for the erratic macroscale friction behaviour seen in the first ~7 mm of sliding, after which point the majority of the shallower wear tracks have disappeared.

As the apex of the SiC sphere wears, gradually flattening and thus reducing in height, it is logical to expect that asperities at the very edge of the interface are steadily introduced into the contact area. Evidence for this are tracks 5, 6 and 7 (Fig. 1c and e), which originate only after several millimetres of sliding. Most prominent is the case of track 7 that appears only during the second sliding stroke. However, the introduction of these asperities into the contact area does not appear to impact the friction response of the macroscale system.

The above experiments and analysis show that the running-in behaviour of this multi-asperity system is very similar to the single asperity response [15,16]. There is evidence of high initial contact pressures and counter surface ploughing, and a transition in the friction and wear mechanism: from the presence of ploughing friction and ploughing wear of the Si flat at the onset of sliding, to a milder wear of the SiC sphere and a lower, more stable friction response once the majority of asperities have been removed. In order to understand the precise wear mechanisms occurring at the asperities themselves, i.e. whether they fracture off in a brittle manner due to structural defects and the high contact pressure at the onset of sliding, or if they wear in a more gradual fashion such as atom-by-atom attrition [29], further investigation is needed. The presence of wear channels on the SiC sphere as explained above do however suggest that a wear mechanism related to asperity fracturing is more likely during running-in, whereby the fractured asperities could subsequently become third bodies able to interact with both the silicon flat and the SiC sphere.

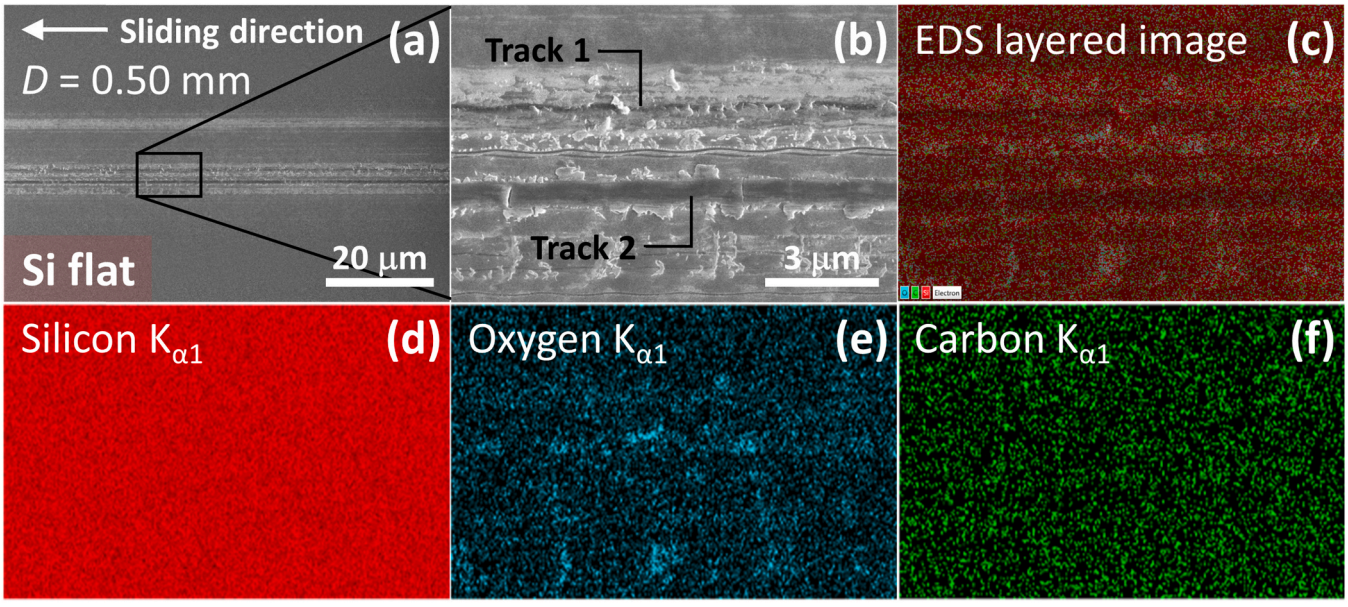

Fig. 2. SEM micrographs showing (a) width of entire wear track on silicon flat after 0.50 mm sliding; (b) magnified region highlighting wear tracks 1 and 2. Corresponding energy dispersive X-ray spectroscopy of magnified region: (c) layered image; (d) silicon $K_{\alpha1}$ signal; (e) oxygen $K_{\alpha1}$ signal; (f) carbon $K_{\alpha1}$ signal.

3.3. Running-in contact simulation

To provide additional validation for the proposed relationship between the wear behaviour of asperities and the macroscale friction response during running-in, elasto-plastic boundary element method (BEM) calculations were performed using AFM surface topography data in Fig. 1d and e as input. The intention was to demonstrate the existence of high initial contact pressures, to trace counter surface wear in relation to single asperity ploughing, and to show further evidence for a transition in the friction and wear mechanism after running-in. In general BEM calculations are a reliable method to assess the contact area, according to the 'Contact-Mechanics Challenge' [26]. Fig. 3 shows the output from BEM calculations of the SiC sphere, illustrating the contact pressure at contacting regions, the area of real contact and average contact pressure prior to and after the running-in period. These calculations reveal that the average contact pressure at the sphere-on-flat interface prior to sliding is high (7.7 GPa) – at least one order of magnitude greater than the Hertzian contact pressure of the system when the surface roughness is not taken into account. In comparison to the sphere condition after running-in, a greater number of contacting asperities prior to sliding exert a contact pressure at the interface high enough to plastically deform the counter surface ($\geq$10 GPa; see Table 1 for Si flat hardness). A distinct transition is demonstrated by the BEM calculation, whereby after running-in, the number of contact points (and the area of real contact) has evidently increased (Fig. 3d and e), yet the contact pressure at the interface has decreased below 10 GPa at almost every contacting position (Fig. 3b). A notable exception is the dominant asperity located at the trailing edge of the SiC sphere, clearly visible in Fig. 3b and c exhibiting a contact pressure $\geq$10 GPa. This finding reinforces the experimental observation that this single asperity is likely responsible for counter surface ploughing track 1, and emphasises the good agreement that exists between experiment and calculation. The high feature in Fig. 1d that develops into SiC asperity '1′ is also visible in Fig. 3a and d, but with fewer contact points exerting a pressure $\geq$10 GPa, indicating that the feature becomes a more dominant ploughing asperity as the sphere surface evolves. The exact regions of the sphere in Fig. 3a that exceed a contact pressure of 10 GPa and could therefore contribute to the formation of ploughing tracks 2–7 on the Si flat, are more challenging to trace. However, there appears a good agreement between the density of the high contact pressure points on the SiC sphere and regions of excess wear debris on the counter surface in Fig. 1c at distance 0.10 mm.

Further utilisation of BEM calculations to trace counter surface wear in relation to single asperity ploughing is displayed in Fig. 4. It shows SEM and AFM micrographs of the Si flat at the beginning and end of the 40 mm unidirectional sliding experiment, and corresponding BEM calculations (utilising AFM surface topography data in Fig. 1d and e as input) predicting the numerical values for the plastic deformation depth (d) into the Si flat, resulting from indentation of the asperities on the harder SiC sphere and assuming a plastic yield stress of 10 GPa for the Si flat. Qualitatively, there appears to be a good agreement between the experimentally-derived asperity positions and those predicted by the BEM calculations to show the plastic deformation on the Si flat; with the width of the wear track at the beginning and end of the sliding experiment also matching closely. However, quantitatively, the correspondence between experiment and model is poor, as the raw numerical

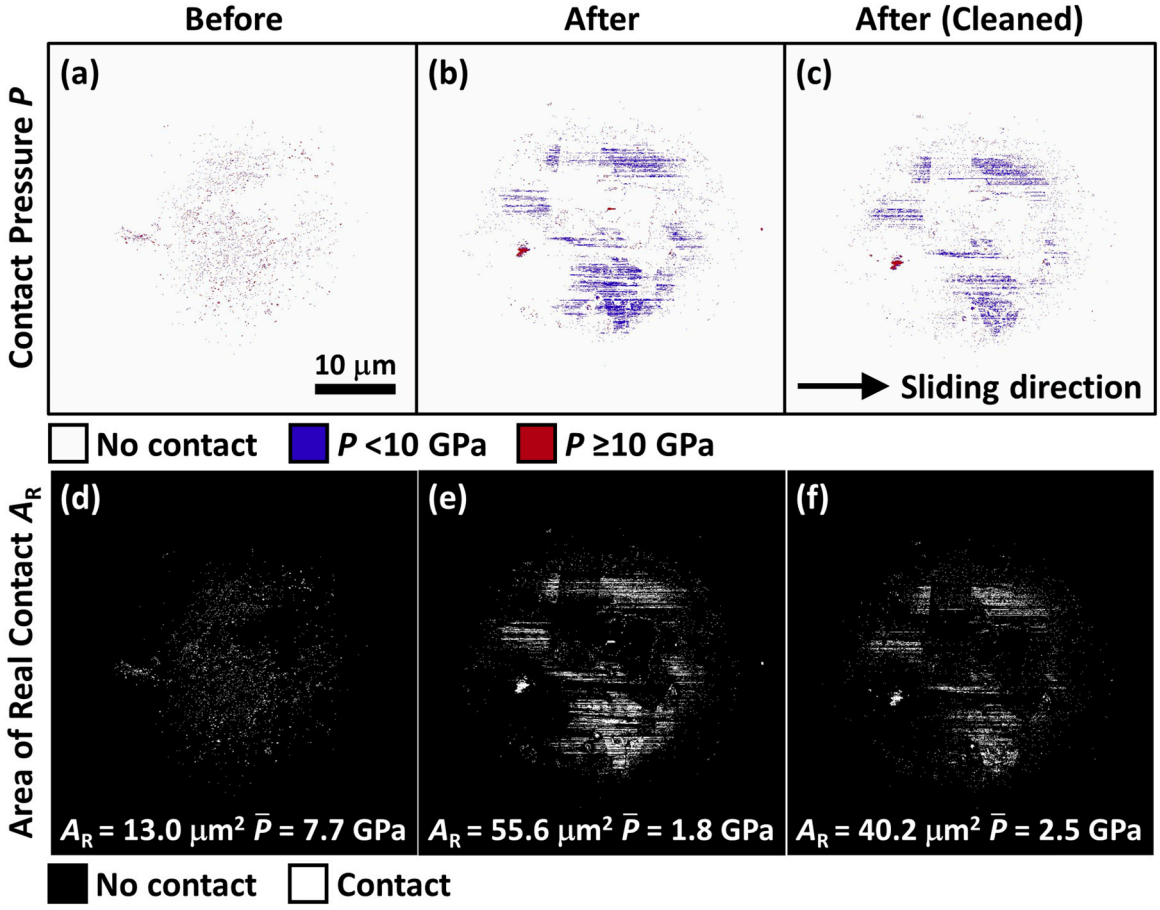

Fig. 3. Boundary element method (BEM) calculations of silicon carbide sphere prior to sliding; after sliding 40 mm; and after sliding and ultrasonic cleaning to illustrate: (a)-(c) the contact pressure (P) at contacting regions on the sphere; (d)-(f) the area of real contact (A_R) and resulting average contact pressure ($\bar{P}$). In all cases a normal force of 100 mN is applied.

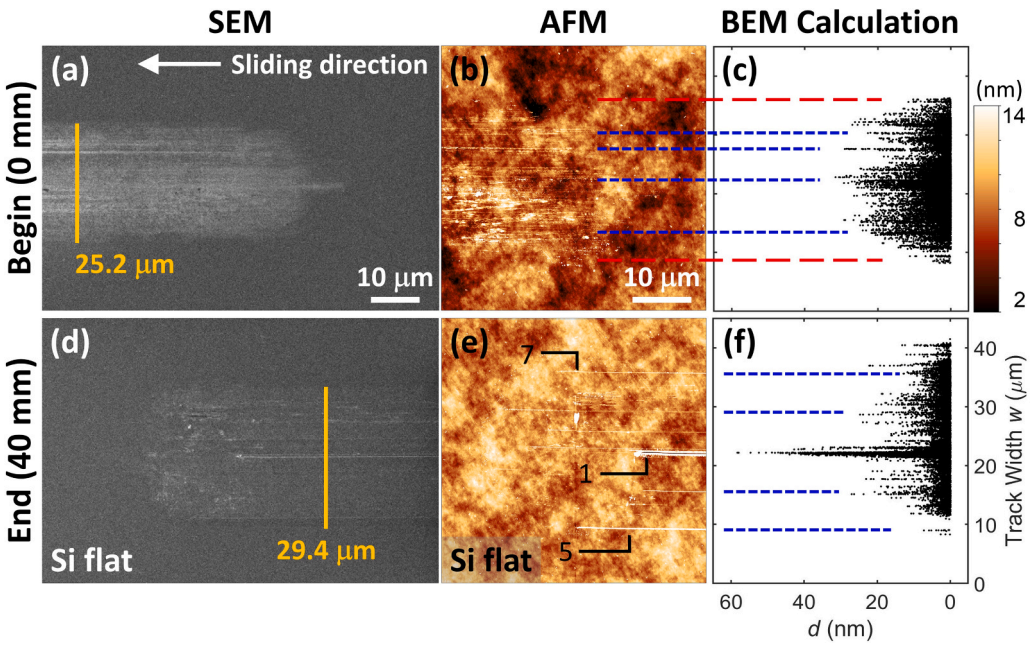

Fig. 4. Tracing silicon (Si) flat wear in relation to silicon carbide (SiC) sphere asperity ploughing prior to and after sliding 40 mm: (a), (d) SEM micrographs of Si flat wear track; (b), (e) AFM micrographs of Si flat wear track. Numbers correspond to possible SiC asperities shown in Fig. 1e and f, assigned responsible for resulting Si flat wear tracks. (c), (f) Boundary element method (BEM) calculations of SiC sphere illustrating the plastic deformation depth (d) of asperities into Si flat.

values for the plastic deformation depth predict initial ploughing tracks approximately 20 nm deep (Fig. 4c), which clearly were not observed experimentally (Fig. 4b). Reasons for this discrepancy will be discussed in more detail in the following section.

A further discrepancy between the BEM predictions and the experimental observations is highlighted when the approximate projected ploughing contact area A_{pr} of each asperity in the sliding direction calculated using the BEM (and displayed in Fig. 4c and f), is used to provide a rough estimate of the expected ploughing force. Ploughing friction F_{pl} for a collection of 'single asperities' can be estimated from the total projected area of contact in the sliding direction with which the asperities plastically penetrate a substrate A_{pr}, multiplied by the hardness of that substrate H_{Si} [30]. The following expression can therefore be used to estimate the CoF due to ploughing at the beginning and end of the 40 mm unidirectional sliding experiment, where F_n is the applied normal force of 100 mN:

$$\mathrm{CoF} = \frac{F_{pl}}{F_n} = \frac{A_{pr} H_{Si}}{F_n} \tag{1}$$

Using this relationship, the calculated CoF resulting from the plastic deformation of the Si flat is 0.12 at the onset of sliding, increasing to 0.21 at the end of the 40 mm unidirectional sliding experiment. Quite clearly there is a large discrepancy between the calculated CoF and the experimental observations, indicating that the reality of the multi-asperity tribological system is much more complex than that based on ploughing of a collection of individual 'single asperities'.

3.4. Discrepancy between experiment and contact simulation

In order to interpret the quantitative differences between the BEM (and ploughing friction) calculation and the experimental results, the running-in friction and wear behaviour of the system is separated into two stages: (i) Onset of sliding after 0.075 mm (where CoF_{max} occurs); (ii) Post running-in at 40 mm.

Considering stage (i) at the onset of sliding or running-in, where the CoF rises to 0.63 after 0.075 mm in the dynamic friction regime, the CoF ought to be predicted by the BEM calculation as this stage is dominated by ploughing friction. However, the CoF calculated by the BEM (0.12) is notably lower than the experimentally derived value. This discrepancy is attributed to the topographical evolution particularly of the Si flat that cannot be captured by the BEM calculation. The high measured CoF at the onset of sliding is accredited to ploughing of the (elevated) Si surface, including the generation, smearing and compression of Si wear debris. In order to verify this reasoning, the ploughing tracks on the Si flat were examined in more detail. SEM and AFM micrographs show that the wear tracks –depicted by regions of light grey and white on the Si flat respectively– are in fact elevated with respect to the background (Fig. 4a, b, d and e). This may be attributed to the formation of SiO_x from Si that has been displaced within the wear tracks. The Pilling-Bedworth (PB) ratio is the ratio of the volume of an oxide to the volume of the metal from which the oxide forms [31]. For oxidation of Si to SiO_2, the PB ratio is approximately 2 [32], meaning that the volume of SiO_2 is twice that of Si, and so effectively causes the volume of material within the wear track to increase. Such an effect cannot be determined by the BEM calculation and potentially explains why the BEM-predicted ploughing tracks of ~20 nm deep (Fig. 4c) were not observed experimentally. However, if the ploughing asperities are at the trailing edge of the sphere, as is the case for those responsible for creating tracks 1 and 2 in Fig. 1, they can generate ploughing tracks that are elevated at the edges but have a centre that is below the background height level of the Si flat. This indicates that with such a 'trailing edge ploughing track', the debris collects next to the track, while other ploughing tracks are potentially covered over. According to the BEM calculations, many of the asperities on the SiC sphere do not result in plastic deformation, but instead exert a contact pressure onto the Si flat that is below the material hardness (Fig. 3) where asperities elastically deform the Si flat. Such asperities can compress the ploughing debris and displace it back into the ploughing track if they come into contact with a track directly after it is formed. This concept is particularly evident in the magnified SEM image in Fig. 2b that shows the elevated wear track, compressed debris and the two distinct 'trailing edge ploughing tracks'.

Further evidence for a high CoF arising as a consequence of ploughing the (elevated) Si surface is shown in Fig. 5. It depicts the friction behaviour of double-stroke 'non-repeated' SiC sphere-on-Si flat friction experiments [27], in which each sliding cycle of the sphere consists of one back-and-forth stroke before the sphere is stepped to a

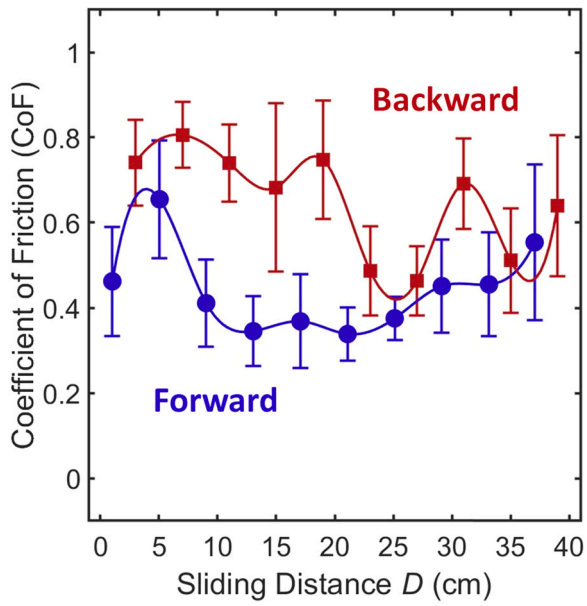

Fig. 5. Coefficient of friction for double stroke 'non-repeated' experiment of a multi-asperity silicon carbide sphere-on-silicon flat over 40 cm sliding distance. All experimental conditions (excluding the sliding mode) identical to that of unidirectional sliding experiment described in this work [27].

fresh area on the Si flat. Fig. 5 clearly shows that the 'backward' stroke sliding over the previously worn track produces a higher friction force than the 'forward' stroke. However, this only occurs during the first 20–25 cm of sliding, when ploughing friction is prominent in the backward stroke. This observation therefore suggests that in such experiments, more ploughing occurs during the backward stroke than the forward stroke. This may seem counterintuitive, as one would not expect ploughing tracks created during the forward stroke to be ploughed again in the backward stroke. However, the observation by SEM and AFM of elevated ploughing tracks suggests that greater ploughing may occur during the backward stroke because the sharpest asperities on the sphere (including asperities that might have otherwise only elastically deformed the flat) will be in contact with this elevated material, thereby penetrating deeper and ploughing over a larger cross section. In fact, it is likely that the aforementioned scenario is already taking place during the forward stroke, when trailing-edge asperities on the SiC sphere slide over the (compressed and elevated) ploughing tracks created by leading-edge asperities. For a single asperity ploughing system, the situation is likely much simpler. The friction force would tend to decrease with the backward stroke, as the single asperity is unlikely to encounter elevated or compressed material as it retraces the ploughing track created during the forward stroke, therefore experiencing less resistance [15,16]. As the BEM can only predict the total CoF in the absence of wear debris and expanded material, the calculated result at stage (i) understandably underestimates the experimental result.

At stage (ii) post running-in at 40 mm, the majority of asperities on the SiC sphere have been removed, and the system has transitioned to one likely dominated by adhesion friction and mild wear of the SiC sphere, where the effect of ploughing as discussed in stage (i) is largely absent except for that generated by trailing edge SiC asperity '1′. The CoF calculated by the BEM (0.21) for the end of the 40 mm unidirectional sliding experiment similarly significantly underestimates the experimentally determined value (0.31). The BEM calculation cannot account for the possible effect wear particles trapped at the sliding interface may have upon the plastic deformation of the Si flat and resulting friction forces. As mentioned above, these wear particles likely originate from asperities at the leading edge of the SiC sphere that have fractured off in the initial sliding strokes, becoming trapped at the contact interface and thus interacting with and wearing both surfaces simultaneously. Evidence for the existence of these wear particles can be found in Fig. 3e and f. The real area of contact on the SiC sphere appears to decrease after cleaning, suggesting that loose and dynamic wear particles were in fact present at the sliding interface. The absence of wear particle dynamic effects is likely to lead to a discrepancy in the calculated CoF, given that the BEM calculations are limited only to one 'snapshot in time'. In addition, the calculated CoF is based only on ploughing friction, and neglects any adhesion friction contribution. The latter is the likely dominating friction mechanism in this regime, originating from smaller interfacial gaps and thus increased area of real contact and lower interfacial contact pressure due to asperity removal, as highlighted by Fig. 3 [27]. Therefore, as the BEM can only partially predict the total CoF, the calculated result at stage (ii) unsurprisingly underestimates the experimentally derived value.

The details presented here highlight that the friction and wear behaviour of a multi-asperity tribological system is much more complex than that of a single asperity system during the running-in process. The BEM can qualitatively predict the locations of the ploughing tracks on the counter surface based upon asperity locations on the sphere, but it cannot predict the degree of plastic deformation of the flat or the resulting friction force due to ploughing. Further work is required in order to fully understand the reasoning behind this quantitative discrepancy, but qualitatively it is evident that the evolution of the counter-surface material (material expansion, compression, trapped wear debris) plays an important role in the friction response of the multi-asperity system. This emphasises the challenges of predicting the friction and wear behaviour of multi-asperity systems on the basis of single asperity contact simulations and scaled-up single asperity system behaviour.

3.5. *Evolution of friction and wear response after running-in at the macroscale*

To understand how the friction and wear behaviour of the multi-asperity SiC-sphere-on-Si flat system evolves after the initial running-in process, a longer unidirectional sliding study over 6 m was conducted. Fig. 6a shows running-in CoF behaviour equivalent to the 40 mm sliding study (Fig. 1b). And consistent with the work reported in [27], for 'non-repeated' reciprocated sliding of brittle non-metallic materials, a steady increase in the CoF is observed over a sliding distance of 6 m. As is highlighted by Fig. 6b-e, the worn contact area of the SiC sphere appears flattened and smoother than the pristine surface, suggesting continuous asperity removal over the course of the 6 m sliding experiment. The wear rate for this system during the running-in process (as presented in Fig. 1) was found to be more than three times that of the overall wear rate for the extended 6 m unidirectional sliding study ($700\ \mu m^3\ (Nm)^{-1}$), providing additional evidence for a transition in the friction and wear mechanism after running-in.

Thus it is likely that the overall steady increase in CoF over the 6 m sliding is not due exclusively to continual asperity ploughing but more conceivably a consequence of adhesion friction following asperity removal, and a gradual increase in area of real contact [27]. This is supported by SEM observations of the wear track on the Si flat. The SEM micrograph inset in Fig. 6a illustrates the topography of the final wear tracks on the Si flat after 6 m sliding and shows no evidence of abrasive wear (unlike the initial sliding track in Fig. 6f) and that the track width has increased to ~60 μm. An estimation can be made to illustrate the potential for adhesion friction and mild wear mechanisms such as atom-by-atom attrition in this multi-asperity tribological system using the method proposed by Hsia et al [27]. This method, without considering strain hardening, is based on the consideration that for rough surfaces, due to asperity-level plastic deformation, the contact pressure in the contact can never become greater than the hardness of the softest material, in this case the Si flat. This sets a minimum limit on the real area of contact, A_{min}. Thus, the minimum number of atoms (inferred as

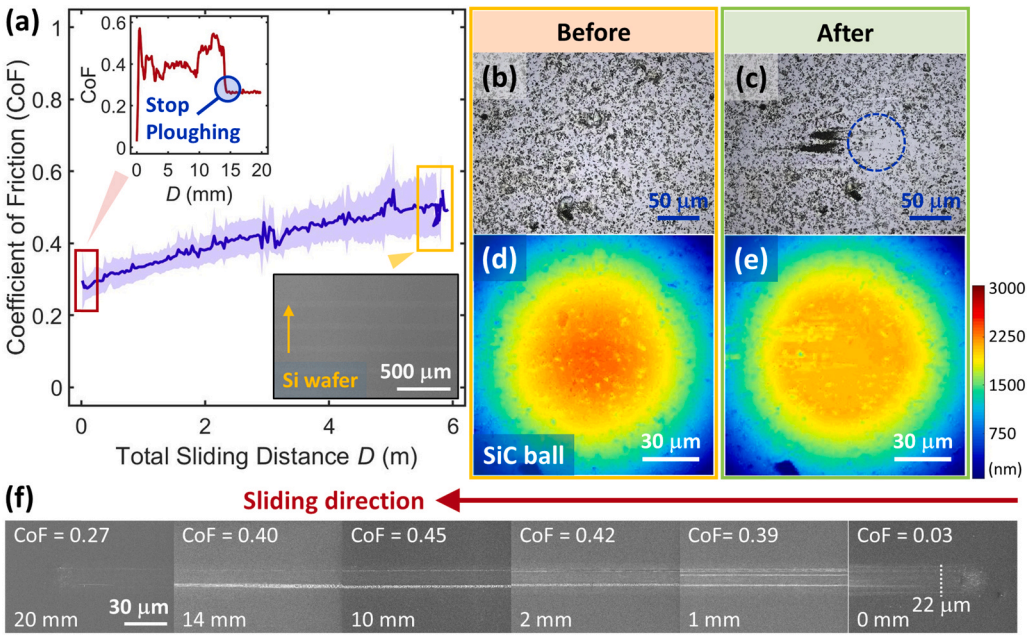

Fig. 6. Friction and wear analysis for unidirectional sliding of a multi-asperity silicon carbide (SiC) sphere-on-silicon (Si) flat over 6 m distance: (a) coefficient of friction (CoF) as a function of sliding distance (solid blue line represents moving average CoF; shaded area represents standard deviation). Upper inset figure shows variation in CoF over initial sliding stroke; Lower inset figure shows SEM micrograph of final wear tracks on Si flat after 6 m sliding. Optical microscopy image of SiC sphere (b) prior to and (c) after sliding. Measured height profile of SiC sphere (d) prior to and (e) after sliding. (f) SEM micrographs of Si flat showing wear track evolution over initial sliding stroke.

an area, A_{min}) on the SiC sphere in contact with the Si flat at any one time during the 6 m unidirectional sliding experiment can be estimated as follows:

$$A_{min} = \frac{F_n}{H_{Si}} = 1.0 \times 10^{-11}\ m^2 \approx \frac{1.0 \times 10^{-11}}{\left(2.0 \times 10^{-10}\right)^2} = 2.5 \times 10^8\ atoms \quad (2)$$

where F_n is the applied normal force (100 mN), H_{Si} is the Si flat hardness (10 GPa) and 2 Å is an approximate atom-to-atom distance. Over the whole area of the contact, 2.5×10^8 atoms on the SiC sphere surface must touch and slide over the Si flat at any time. Thus, using the total wear volume (4.2×10^{-16} m^3) measured from the height profile in Fig. 6e, it is possible to estimate the number of atoms removed from the SiC sphere surface over the 6 m sliding distance and thus the average distance required to remove one atomic layer:

$$\frac{4.2 \times 10^{-16}}{\left(2.0 \times 10^{-10}\right)^3} \approx 5 \times 10^{13} atoms \text{ removed} \quad (3)$$

$$\frac{6\ m \times 2.5 \times 10^8}{5 \times 10^{13}} \approx 30\ \mu m \quad (4)$$

This approximation indicates that the atoms on the SiC surface that make contact with the Si flat slide an average of at least 30 µm (a distance that is equivalent to more than one hundred thousand atomic spacings) before one atomic layer is worn off. As there is evidence to suggest plastic deformation of the Si flat and asperity removal on the SiC sphere and thus a higher wear rate during the running-in process, the above calculation is likely to underestimate the mildness of the subsequent wear occurring at the SiC sphere-on-Si flat interface. This in itself provides additional support for atom-by-atom wear [10,33], and adhesion friction being the dominant mechanism once the ploughing-asperity removal transition point has occurred.

As for the nature of the atomic attrition-like wear mechanism, it is plausible that a mechanochemical process is occurring at the SiC sphere-on-Si flat interface. As a unidirectional sliding mode was used, the SiC sphere continuously made contact with 'fresh' unworn native oxide layer on the Si flat. The bond energies (enthalpies) of the native oxide layer Si–O (452 kJ mol^{-1}), O–H (459 kJ mol^{-1}) and any potentially formed interfacial bonds O-C (358 kJ mol^{-1}) are all greater than that of Si–C (318 kJ mol^{-1}) [34]. Therefore, the probability that a Si–C bond would break before an O–H or Si–O, or indeed any interfacial O–C bonds, is higher. Hence, chemically, there is a preference for the removal of atoms one-by-one from the SiC sphere – which is in essence atomic attrition [10,33].

4. Conclusion

The running-in wear mechanisms of multi-asperity contacts were investigated at the micro- and nanoscale in relation to the friction behaviour of a macroscale tribological system sliding in a unidirectional mode. Focus was placed upon the study of industrially-relevant silicon carbide and silicon materials; systems with a Hertzian contact pressure less than that of the hardness of the contacting bodies. Experimental methods and contact simulations were combined in order to study the multi-asperity interfaces at a level of detail of a single asperity, as the system transitioned through the initial running-in stage. The resulting friction response of such a tribological system was found to be initially high and erratic at the onset of sliding, with a rapid decline to a stabilised friction coefficient after ~15 mm running-in period. Thereafter, the friction coefficient was observed to increase relatively steadily over a total sliding distance of 6 m.

A direct correlation was found between the friction behaviour from 0 to 15 mm, the appearance and disappearance of ploughing tracks on the flat, and the simultaneous removal of asperities on the sphere. It was understood that the macroscale friction response during the running-in period was likely dominated by ploughing wear at a high wear rate, originating from the very high contact pressure exerted beneath the asperities at the sphere-on-flat interface. The behaviour observed for this multi-asperity system, although more erratic, followed that of single asperity running-in friction behaviour reported in the literature. Contrary to a single asperity system however, the evolution of the counter-surface material (material expansion, compression, trapped wear debris), was found to play a dominant role in the friction response of the multi-asperity system; emphasising the challenges associated with potential scale-up theories.

A transition point in the wear mechanism of the multi-asperity system appeared to occur once the majority of asperities were removed. In line with the steady increase in friction observed over the remaining 6 m; the average contact pressure at the interface was seen to decrease, thus lowering the wear rate as the real area of contact gradually increased. On average the rate of material removal was very low,

occurring at an atomic attrition-like rate that is potentially attributed to adhesive wear involving mechanochemical reactions on an atomic scale. Overall, the friction behaviour of this multi-asperity brittle non-metallic tribological system appears to be governed by the wear behaviour of the asperities, and the influence their existence has upon the interfacial contact pressure.

CRediT authorship contribution statement

Feng-Chun Hsia: Conceptualization, Methodology, Validation, Formal analysis, Investigation, Writing – review & editing, Visualization. **Fiona M. Elam:** Conceptualization, Methodology, Formal analysis, Investigation, Writing – Original Draft, Writing – review & editing. **Daniel Bonn:** Resources, Writing – Review & Editing. **Bart Weber:** Conceptualization, Writing – review & editing, Supervision, Funding acquisition. **Steve E. Franklin:** Conceptualization, Writing – review & editing, Supervision.

Declaration of Competing Interest

The authors declare that they have no known competing financial interests or personal relationships that could have appeared to influence the work reported in this paper.

Acknowledgements

This work has been carried out at the Advanced Research Center for Nanolithography (ARCNL), a public-private partnership of the University of Amsterdam (UvA), the Vrije Universiteit Amsterdam (VU), the Netherlands Organisation for Scientific Research (NWO) and the semiconductor equipment manufacturer ASML. The authors would like to thank Arend-Jan van Calcar (ARCNL) for his technical assistance. B.W. acknowledges funding from the NWO VENI Grant No. VI.Veni.192.177.

References

[1] Holmberg K, Erdemir A. Global impact of friction on energy consumption, economy and environment. FME Trans 2015;43:181–5. https://doi.org/10.5937/fmet1503181H.
[2] Holmberg K, Erdemir A. Influence of tribology on global energy consumption, costs and emissions. Friction 2017;5:263–84. https://doi.org/10.1007/s40544-017-0183-5.
[3] Grabon W, Koszela W, Pawlus P, Ochwat S. Improving tribological behaviour of piston ring-cylinder liner frictional pair by liner surface texturing. Tribol Int 2013;61:102–8. https://doi.org/10.1016/j.triboint.2012.11.027.
[4] Tyfour WR, Beynon JH, Kapoor A. The steady state wear behaviour of pearlitic rail steel under dry rolling-sliding contact conditions. Wear 1995;180:79–89. https://doi.org/10.1016/0043-1648(94)06533-0.
[5] Luck DL, de Boer MP, Ashurstl WR, Baker MS Evidence for pre-sliding tangential deflections in MEMS friction. TRANSDUCERS 2003 - 12th Int. Conf. Solid-State Sensors, Actuators Microsystems, 2003, p. 404–7. ⟨https://doi.org/10.1109/SENSOR.2003.1215339⟩.
[6] Greco A, Sheng S, Keller J, Erdemir A. Material wear and fatigue in wind turbine Systems. Wear 2013;302:1583–91. https://doi.org/10.1016/j.wear.2013.01.060.
[7] Stoyanov P, Chromik RR. Scaling effects on materials tribology: From macro to micro scale. Mater (Basel) 2017;10:550. https://doi.org/10.3390/ma10050550.
[8] Blau PJ. Friction science and technology: From concepts to applications. 2nd ed. Boca Raton, FL: CRC Press; 2008.
[9] Blau PJ. On the nature of running-in. Tribol Int 2005;38:1007–12. https://doi.org/10.1016/j.triboint.2005.07.020.
[10] Jacobs TDB, Carpick RW. Nanoscale wear as a stress-assisted chemical reaction. Nat Nanotechnol 2013;8:108–12. https://doi.org/10.1038/nnano.2012.255.
[11] Zhao K, Aghababaei R. Interfacial plasticity controls material removal rate during adhesive sliding contact. Phys Rev Mater 2020;4:103605. https://doi.org/10.1103/PhysRevMaterials.4.103605.
[12] Bhaskaran H, Gotsmann B, Sebastian A, Drechsler U, Lantz MA, Despont M, Jaroenapibal P, Carpick RW, Chen Y, Sridharan K. Ultralow nanoscale wear through atom-by-atom attrition in silicon-containing diamond-like carbon. Nat Nanotechnol 2010;5:181–5. https://doi.org/10.1038/nnano.2010.3.
[13] Gotsmann B, Lantz MA. Atomistic wear in a single asperity sliding contact. Phys Rev Lett 2008;101:125501. https://doi.org/10.1103/PhysRevLett.101.125501.
[14] Reitsma MG, Cain RG, Biggs S, Smith DW. Wear of a single asperity using Lateral Force Microscopy. Tribol Lett 2006;24:257–63. https://doi.org/10.1007/s11249-006-9154-0.
[15] Schiffmann KI, Hieke A. Analysis of microwear experiments on thin DLC coatings: friction, wear and plastic deformation. Wear 2003;254:565–72. https://doi.org/10.1016/S0043-1648(03)00188-1.
[16] Yu J, Hu H, Jia F, Yuan W, Zang H, Cai Y, Ji F. Quantitative investigation on single-asperity friction and wear of phosphate laser glass against a spherical AFM diamond tip. Tribol Int 2015;81:43–52. https://doi.org/10.1016/j.triboint.2014.07.020.
[17] Bhushan B, Nosonovsky M. Comprehensive model for scale effects in friction due to adhesion and two- and three-body deformation (plowing). Acta Mater 2004;52:2461–74. https://doi.org/10.1016/j.actamat.2004.01.038.
[18] Roscioli G, Taheri-Mousavi SM, Tasan CC. How hair deforms steel. Science 2020;369:689–94. https://doi.org/10.1126/science.aba9490.
[19] Khurshudov AG, Kato K, Koide H. Wear of the AFM diamond tip sliding against silicon. Wear 1997;203–204:22–7. https://doi.org/10.1016/S0043-1648(96)07447-9.
[20] Fletcher PC, Felts JR, Dai Z, Jacobs TD, Zeng H, Lee W, Sheehan PE, Carlisle JA, Carpick RW, King WP. Wear-resistant diamond nanoprobe tips with integrated silicon heater for tip-based nanomanufacturing. ACS Nano 2010;4:3338–44. https://doi.org/10.1021/nn100203d.
[21] Yu B, He H, Chen L, Qian L. Tribological behavior of monocrystalline silicon from single- to multiple-asperity scratch. Wear 2017;374–375:29–35. https://doi.org/10.1016/j.wear.2016.11.040.
[22] Qi H, Hu W, He H, Zhang Y, Song C, Yu J. Quantitative analysis of the tribological properties of phosphate glass at the nano- and macro-scales. Friction 2020. https://doi.org/10.1007/s40544-020-0411-2.
[23] Krick BA, Vail JR, Persson BNJ, Sawyer WG. Optical in situ micro tribometer for analysis of real contact area for contact mechanics, adhesion, and sliding experiments. Tribol Lett 2012;45:185–94. https://doi.org/10.1007/s11249-011-9870-y.
[24] Garabedian NT, Bhattacharjee A, Webster MN, Hunter GL, Jacobs PW, Konicek AR, et al. Quantifying, locating, and following asperity-scale wear processes within multiasperity contacts. Tribol Lett 2019;67:89. https://doi.org/10.1007/s11249-019-1203-6.
[25] Bhushan B. Nanotribology and nanomechanics of MEMS/NEMS and BioMEMS/BioNEMS materials and devices. Micro Eng 2007;84:387–412. https://doi.org/10.1016/j.mee.2006.10.059.
[26] Müser MH, Dapp WB, Bugnicourt R, Sainsot P, Lesaffre N, Lubrecht TA, et al. Meeting the contact-mechanics challenge. Tribol Lett 2017;65:118. https://doi.org/10.1007/s11249-017-0900-2.
[27] Hsia F-C, Elam FM, Bonn D, Weber B, Franklin SE. Wear particle dynamics drive the difference between repeated and non-repeated reciprocated sliding. Tribol Int 2020;142:105983. https://doi.org/10.1016/j.triboint.2019.105983.
[28] Necas D, Klapetek P. Gwyddion: an open-source software for SPM data analysis. Cent Eur J Phys 2012;10:181–8. https://doi.org/10.2478/s11534-011-0096-2.
[29] Bernal RA, Carpick RW. Visualization of nanoscale wear mechanisms in ultrananocrystalline diamond by in-situ TEM tribometry. Carbon N Y 2019;154:132–9. https://doi.org/10.1016/j.carbon.2019.07.082.
[30] Liefferink RW, Weber B, Bonn D. Ploughing friction on wet and dry sand. Phys Rev E 2018;98:052903. https://doi.org/10.1103/PhysRevE.98.052903.
[31] Pilling NB, Bedworth RE. The oxidation of metals at high temperatures. J Inst Met 1923;29:529–82.
[32] Matsuda T, Inami K, Motoyama K, Sano T, Hirose A. Silver oxide decomposition mediated direct bonding of silicon-based materials. Sci Rep 2018;8:10472. https://doi.org/10.1038/s41598-018-28788-x.
[33] Liu J, Jiang Y, Grierson DS, Sridharan K, Shao Y, Jacobs TDB, Falk ML, Carpick RW, Turner KT. Tribochemical wear of diamond-like carbon-coated atomic force microscope tips. ACS Appl Mater Interfaces 2017;9:35341–8. https://doi.org/10.1021/acsami.7b08026.
[34] King RB, editor. Encyclopedia of inorganic chemistry. 2nd ed. John Wiley & Sons Ltd; 2006. https://doi.org/10.1002/0470862106.id098.